remote sensing

MDPI

Article

Quantifying Changes in Extent and Velocity of the Hornbreen/Hambergbreen Glacial System (SW, Spitsbergen) Based on Timeseries of Multispectral Satellite Imagery

Dawid Saferna *, Małgorzata Błaszczyk, Mariusz Grabiec and Bogdan Gądek

Institute of Earth Sciences, Faculty of Natural Sciences, University of Silesia in Katowice, Bedzinska 60, 41-200 Sosnowiec, Poland; malgorzata.blaszczyk@us.edu.pl (M.B.); mariusz.grabiec@us.edu.pl (M.G.); bogdan.gadek@us.edu.pl (B.G.)

* Correspondence: dawid.saferna@o365.us.edu.pl

Abstract: This study focuses on the Hornsund region in Svalbard, where the temperature has risen by 1.14 °C per decade, six times faster than the global average. The accelerating temperature rise in the Arctic has had significant impacts on the Svalbard glaciers, including the Hornbreen–Hambergbreen system (HH system). The HH system connects Sørkapp Land with the rest of Spitsbergen, and its disintegration will lead to the formation of a new island. This study assesses the annual and seasonal changes in the velocity of the HH system and fluctuations of the position of the termini from 1985 to 2021 and their relationship with environmental factors. Furthermore, an assessment was made of the possible date of opening of the Hornsund strait. The study also investigates the impact of the radiometric resolution of satellite images on the quality of the velocity field and the detection of glacier features. Multispectral imagery was used to assess the velocity fields with Glacier Image Velocimetry (v 1.01) software, which uses the feature tracking method. In addition, the Glacier Termini Tracking plugin was used to acquire data on the fluctuating positions of the termini. The long-term mean annual velocity of the Hornbreen was 431 m a^{-1}, while that of Hambergbreen was 141 m a^{-1}. The peak seasonal velocity and fluctuations of the terminus position of Hambergbreen were delayed by approximately one month when compared to Hornbreen. Overall, air and sea surface temperatures influence the velocities and fluctuations of the termini, while precipitation plays a secondary role. If the recession continues, the Hornsund strait may open around 2053. An increase in the quality of velocity maps from 12.7% to 50.2% was found with an increase in radiometric resolution from 8 bit to 16 bit.

Keywords: glacier velocity; Hornsund; Hornbreen; Hambergbreen; feature tracking; satellite imagery; radiometric resolution

Citation: Saferna, D.; Błaszczyk, M.; Grabiec, M.; Gądek, B. Quantifying Changes in Extent and Velocity of the Hornbreen/Hambergbreen Glacial System (SW, Spitsbergen) Based on Timeseries of Multispectral Satellite Imagery. *Remote Sens.* **2023**, *15*, 3529. https://doi.org/10.3390/rs15143529

Academic Editor: Yi Luo

Received: 31 May 2023
Revised: 7 July 2023
Accepted: 11 July 2023
Published: 13 July 2023

1. Introduction

The temperature in the Arctic is rising three times faster than the global average [1]. This is evident in the Hornsund region (South Spitsbergen, Svalbard), where the annual temperature has increased by 1.14 °C per decade (six times faster than the global average) during the 1979–2018 period [2]. Ongoing warming has impacts on the velocity and recession of the Svalbard glaciers [3,4]. It also leads to the transformation of the landscape (e.g., the creation of new islands) [5].

The Hornbreen–Hambergbreen glacier system (HH system) (Figure 1) is a natural border between the Greenland Sea and the Barents Sea. Further deglaciation of the HH system will separate Sørkapp Land from the rest of Spitsbergen. In the 1960s, a hypothesis was presented, in which the location of the bed of the HH system lay below sea level [6]. The hypothesis was further discussed in several studies [7–10]. In 2013–2014, ground penetrating radar (GPR) surveys finally proved the continuous subsea overdeepening of the glacier bed [11] and the possibility that the strait could open up in the near future.

Subsequent research has shown the following approximations of the final deglaciation date of the HH system: the end of 20th century [6,7], 2020 [8], 2030–2035 [9], and 2055–2065 [11]. Opening the strait between Sørkapp Land and Torell Land may result in a significant change in the local ecosystem [9,11] and may create a new marine route. The long-term retreat of both glaciers was described by Blaszczyk et al. [3], Grabiec et al. [11], and Kavan et al. [12]. The retreat was interrupted by surges, leading to an increase in their extent and velocity [11]. However, previous research on the retreat rate of the Hornsund glaciers often lacks an analysis of seasonal variations. A complex study of the seasonal fluctuations of glacier fronts and their linkage to environmental factors has only been conducted for Hornsund [13] (especially on Hansbreen [14]); therefore, the focus has been placed on the HH system.

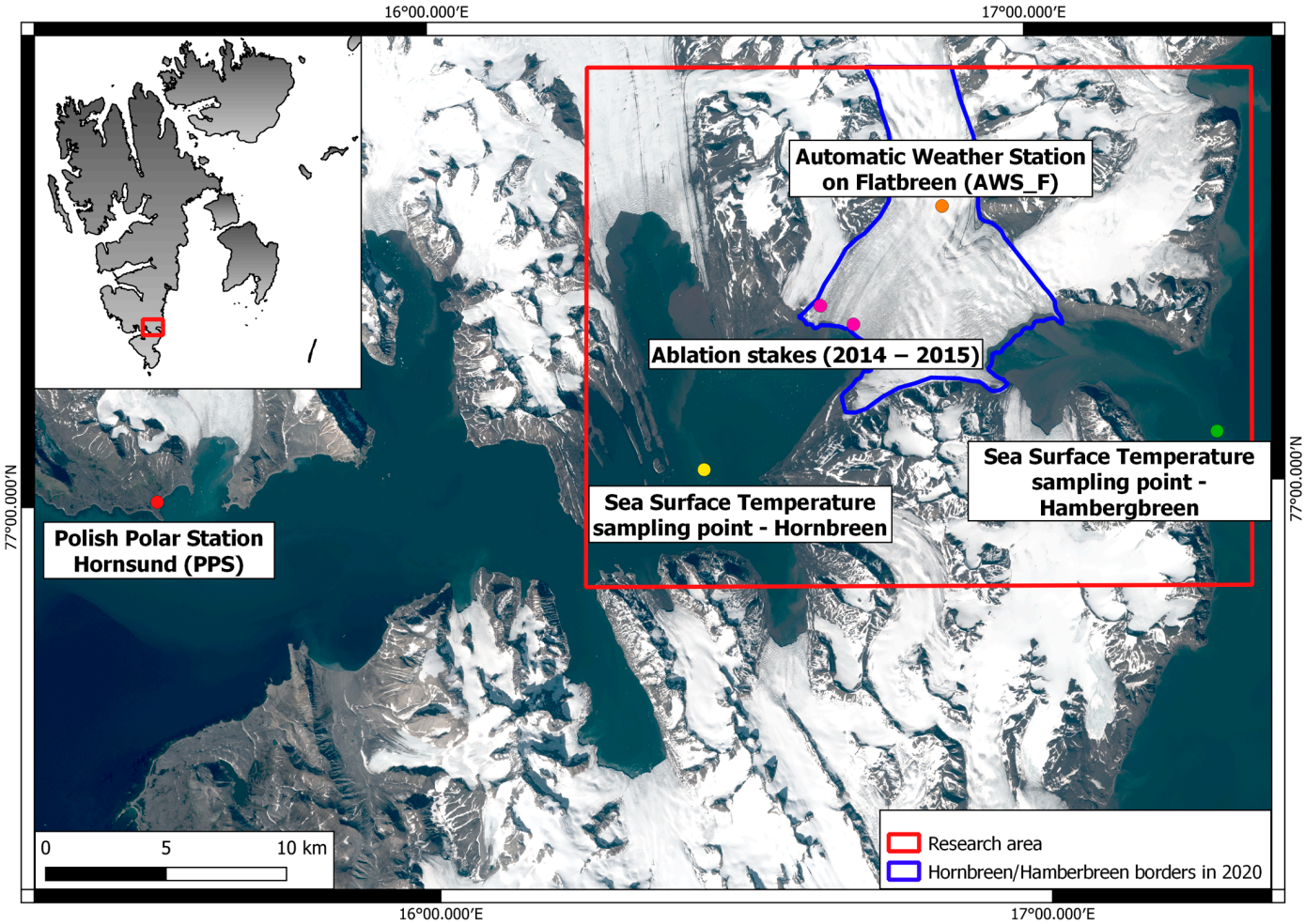

Figure 1. Study area, its position on the Svalbard map, and data acquisition points.

In polar regions, remote sensing methods are frequently used as an alternative to time-demanding and weather-dependent in situ measurements. The remote sensing-based feature tracking method can efficiently assess glacier surface velocity [15,16]. Velocity assessment using data from optical sensors cannot be conducted during the polar night, in contrast to radar data that can be used in all weather conditions and in the absence of daylight. Some databases offer feature tracking-based velocity maps. The MEaSUREs ITS_LIVE project, run by NASA, has provided global velocity and elevation data since 1985 [17]. The dataset is mainly based on Landsat missions and has considerable data gaps (especially before 2012 and in the polar night). The RETREAT repository contains annual and monthly data from October 2014 to January 2022 [18]. Velocity mosaics are based on optical and radar data (e.g., Sentinel 1, TerraSAR-X). Overall, the ITS_LIVE database is not

appropriate for this study (especially for data older than 2012), and RETREAT's time range is very limited.

This study aims to assess annual and seasonal changes in the dynamics of the HH system over the period 1985–2021. Due to a lack of continuity between the ITS_LIVE and RETREAT databases and a lack of ITS_LIVE data before 2012, these databases were not used so that a common methodology could be maintained and velocities could be calculated independently. Optical imagery (Landsat 4–8, ASTER, Sentinel 2) was used to analyse fluctuations of the termini and velocities. To investigate their relationships with environmental factors, the results were compared with air temperature, sea surface temperature, and precipitation. In this study, the deglaciation rate of the HH system and the Sørkapp Land separation date were also estimated.

Furthermore, an investigation was made on the influence of the technical properties (e.g., spatial resolution) of satellite images on the quality of the velocity field. The recognition of features on glacier surfaces (e.g., crevasses, supraglacial streams) is essential in the feature tracking method. The spatial resolution of satellite imagery is one of the most important factors influencing the possibility of the detection of features [19,20], but pixel depth (radiometric resolution) also matters [21,22]. Radiometric resolution is the ability of distinguishing between two similar but not identical radiances [20]. In this paper, the influence of radiometric resolution on the data quality of the feature tracking output was investigated.

2. Study Area

The HH system is located in Hornsund fiord, South Spitsbergen (Figure 1). Glaciers fill the depression between Torrel Land and Sørkapp Land and separate the Greenland and Barents seas [23]. Hambergbreen is located on the east side of the research area; it covers 16.6 km^2 [12]; and its terminus is 5.6 km wide. Up until 2009, Hambergbreen was also connected to Sykorabreen. Hornbreen is located on the west side of the HH system and has a 4 km wide terminus; it covers a total area of 176.2 km^2 [3]. Flatbreen and Skjoldfonna now feed the HH system. The glacier bed of HH lies 40 m below sea level (71.2 m.b.s.l at the deepest point) and the maximum ice thickness in those parts of the glaciers investigated was 261 m [11]. The mean surface slope of Hornbreen is 1.3° [3], while the surface slope under the HH connection varies between 0.5° and 0.7° [11].

HH is a polythermal glacier with a significant predominance of temperate ice [11]. Due to a decrease in the area of Firn, the cold ice may expand [24]. At the end of the Little Ice Age, both glaciers were at their maximum extent. Surges occurring at that time pushed the terminus of the Hambergbreen far into the Barents Sea and the ice masses to the southern border of the ice bridge. Since then, the glaciers have been in recession, interrupted by surges (Hornbreen~1930, Hambergbreen/Sykorabreen~1960, 1980) [9–11,25,26]. The mean retreat rate of Hornbreen since 1899 is 130 m a^{-1} [9,11], while that of Hambergbreen in the 1970–2019 period was 149 m a^{-1} [12].

The climate in the Hornsund area is classified as Tundra climate (a subtype of polar climate) [27]. The mean annual air temperature in 1979–2020 was −3.6 °C [28] and rose by 1.14 °C/decade [2]. The winter season is seen to be warming faster than summer [2] and the duration and frequency of winter thaws are increasing [29]. The horizontal thermal gradient in southern Spitsbergen rises from E to W [30,31], and the increase in air temperature is linked to the warming of sea currents [32]. The west side of the HH system is influenced by the warm West Spitsbergen Current, while the east side is affected by the cold current from the Barents Sea [23,30]. The warming of these water masses is called atlantification and is particularly visible on the west side of Spitsbergen [33]. Precipitation in the Hornsund area is relatively high [2] and reached an annual value of 466.1 mm/year in 1979–2020 [28], showing an increasing trend of 61.6 mm/decade [2]. The highest precipitation occurs in September, while the lowest is in April [2].

3. Data and Methods

The optical imagery and environmental data used to estimate velocity and changes to the glacier termini are presented in this section. In addition, a presentation is also made of the software and the methods with which the analysis and assessment of velocity quality and its dependence on the radiometrical resolution of satellite data were conducted.

3.1. Optical Imagery

Satellite images used to calculate the glacier velocities and extent were delivered by sensors specified and described in Table 1.

Table 1. Selected parameters of the satellite images used; *—the radiometric resolution of the imagery acquired is 12 bit, but data are provided as 16 bit.

Satellite	Bands Used	Spatial Resolution (m)	Radiometric Resolution (bits)	Number of Images	Time Span
Landsat 5	1–7	30	8	56	27 May 1985–27 September 1998
Landsat 7	8	15	8	16	27 July 1999–12 July 2002
ASTER	3N/B	15	8	25	23 June 2001–15 August 2012
Landsat 8	8	15	16	14	22 March 2014–31 July 2015
Sentinel 2	2–4, 8	10	12 (16) *	47	1 April 2016–27 September 2021

The images cover the period from May 1985 to September 2021, with limited availability in 2001–2014 and a lack of data during polar nights. In total, 129 images have been applied and formatted into .tiff and .hdf. The minimum interval of image acquisition was two weeks and the maximum was three years (it was impossible to calculate velocity with this pair). Despite being georeferenced (UTM 33X), the position of images was sometimes incorrect (error up to 10 km in the case of Landsat 5). To resolve the positioning problem, all images were manually referenced with the fixed points located within the image range (e.g., peaks, stones, moraines, shoreline).

3.2. Sea Surface Temperature (SST)

SST data were retrieved from the "Sea surface temperature daily data from 1981 to present derived from satellite observations" resource managed by the European Space Agency and Copernicus Climate Change Service [34]. The dataset includes daily SST at a 20 cm water depth during the entire study period. SST was based on infrared measurements conducted by multiple sensors: advanced very high-resolution radiometers (AVHRRs), along-track scanning radiometers (ATSRs), and a sea and land surface temperature radiometer (SLSTR). Interpolated and validated data are available in $0.05^\circ \times 0.05^\circ$ spatial resolution [34–37]. Validation shows that values of SST determined from satellite data at high latitudes are lower than in situ measurements [34]. Data were converted to GeoTIFF and sampled from points located in front of the positions of the termini (Figure 1). SSTs measured near the entrance of Hornsund fiord were validated with CTD probe (conductivity, temperature, depth) data collected in the period 2011–2015 [14,38]. Here, a comparison was made between CTD temperatures at 20 cm depth and SST data. The correlation was $r = 0.93$ ($p = 0.001$) and the mean temperature difference was 0.64 °C (in situ measurements were, in most cases, lower than satellite measurements).

3.3. Climatic Data

Daily air temperature and precipitation data at the Polish Polar Station (PPS) for the period 1985–2019 were collected from PANGEA [39]. The final period (2020–2021) was completed with data from bulletins published by PPS [40]. The PPS station lies at 10 m.a.s.l, 300 m from the shore of Isbjornhamma and 30 km from the HH system. PPS meteorological monitoring includes both information from AWS (Automatic Weather Station) data and manual observations by scientific staff [41]. Additionally, the daily, monthly, and annual

sums of PDD (positive degree days) were calculated as well as the rainfall totals. The rainfall totals were estimated as the sum of all precipitation values when the air temperature exceeded 0 °C. PPS air temperature data were correlated with data from AWS_F mounted on the Flatbreen glacier (Figure 1) situated in the upper section of Hornbreen [42]. AWS_F (N77°06′ E16°50′, 186 m.a.s.l) operated for nearly one year (20 April 2013–5 April 2014). The correlation coefficient between PPS and AWS_F temperatures was r = 0.97 (p = 0.001). The mean difference between PPS and AWS_F temperature records was 3.2 °C with colder weather conditions on the eastern side of the fiord caused by the cold East Spitsbergen Current [30,31].

3.4. Glacier Velocity Calculations

To estimate the velocities of the study glaciers, glacier image velocimetry (GIV) [19], a MATLAB script that uses the feature tracking method, was used. This technique has been used in glaciological applications since the 1990s [15,16] and has been used in many varied tools [19].

Satellite data that consist of more than one spectral band were processed into one layer with the mean value of all the bands used. Pairs used to calculate average velocities during the polar night consist of the last available optical image from the previous year and the first available image of the following year. In most cases, polar night velocities could not be calculated because there was too long a gap between the acquisition of images, as intense changes in the surface prevents the algorithm from recognising the same surface features. The application resamples all satellite data to a common resolution and then searches for correlation in subsequent pairs of images. All characteristic shapes in reference chips (e.g., crevasses, boulders, medial moraines, supraglacial channels, foliation) are sought around search chips. The cross-correlation algorithm provides information about displacement direction and distance, which is divided by the time difference between the acquisition dates of the image pair.

In addition to at least one pair of images, the application requires additional files: mask—the borders of glaciers being investigated in RGB 0,0,0; save the image—a background image on which output data will be presented; and stable—an optional file which contains stable ground in RGB 0,0,0 and in particular is used for slow-moving glaciers to calibrate output data. Pre-processing settings consist of two built-in filters to improve the detectability of characteristic features. Near anisotropic orientation filter (NAOF) is a variation of the orientation filter [43] that significantly improves the visibility of features in cloudy images. An intensity cap filter was also used to reach better contrast, which provided better matches in cross-correlation processing.

Output GeoTIFF files that contain monthly velocities were visually validated, and the rasters with clearly visible artefacts in the frontal parts of glaciers were removed. To estimate velocities near the front and eliminate noise that could interrupt further analysis, the data investigated were limited to polygons extending up to 500 m from the termini. Finally, the median of the velocity values within the polygons that had been drawn was calculated. This value was used in further analysis as the monthly/annual velocities.

To validate our results, the output GeoTIFF were compared with ablation stake data mounted on Hornbreen [44,45]. Ablation stake data included annual velocity data from the 2014–2015 period (Figure 1).

3.5. Estimating Changes in the Position of the Termini

To estimate changes in the position of the glacier termini, the same optical imagery dataset was used for the velocity calculations. The glacier termini tracking (GTT) toolbox [46] contains three tools for the two-dimensional determination of changes in glacier extent.

GTT uses vectorised positions of the termini in layers with attributes that contain the date of acquisition of the terminus position, glacier direction relative to the terminal line, and glacier name. The algorithm creates points along vector layers and links corresponding points. The final result is a spreadsheet containing the front position change statistics based

on the vectorised links between points. Statistics estimated in this study included the mean, median, max, and min values as well as the standard deviation of the change of terminus position. Finally, mean changes between the positions of the termini were converted to monthly values. Such an approach is essential in studying wide fluctuations in the position of the glacier terminus when a section of the front is advancing, while at the same time, another section is retreating.

The last stage of the research was the supposed date of their disintegration. The distances between the positions of the termini were measured in September 2021 and the point of intersection of the centrelines of the Hornbreen, Hambergbreen, and Flatbreen subglacial reliefs were identified. Then, these distances were divided by the mean annual retreat rate of glaciers.

3.6. Influence of Radiometric Resolution on Velocity Data

To assess the importance of different radiometric resolutions on velocity data, annual velocity maps based on imagery from four different sensors were visually compared. For this, 8-bit and 16-bit satellite data were used. The time spans of the imagery used, as well as the number of images, are included in Table 1.

To quantify the impact of pixel depth on the feature tracking-based velocity maps, the velocity was computed separately for four pairs of images from two sensors (Landsat 8, Sentinel 2) with (winter) and without (summer) snow cover. Only satellite images provided with 16-bit resolution were used here. Information about the dates of acquisition of images along with information about the sensors is included in Table 2. To assess the quality of the velocities generated depending on pixel depth, 16-bit data were downgraded into 8-bit resolution. In addition, output data were reclassified into three unique classes. Values lower than three times the distance of the standard deviation from the mean cell value are classified as correct values. Outliers were defined as all values that are higher than three times the distance of the standard deviation from the mean cell value. The mean and standard deviation values were based on 2015–2021 data (best quality), the cell statistic tool in Quantum GIS was used to assess this statistical indicator. All outliers were recognised as noise; no data cells were assigned as third class. No data cells are the consequence of too low a similarity between the reference and search chips. The last step was a comparison of the default and downgraded reclassified output rasters.

Table 2. Selected parameters of satellite imagery used for the investigation of the importance of spatial resolution in the feature tracking method; *—radiometric resolution of the imagery acquired is 12 bit, but the data are provided at 16 bits.

Season	Sensor	Date of Acquisition	Spatial Resolution (m)	Radiometric Resolution (Bits)
Summer	Landsat 8	6 August 2014 22 August 2014	15	16
	Sentinel 2	11 July 2021 10 August 2021	10	12 (16) *
Winter	Landsat 8	3 April 2015 3 May 2015	15	16
	Sentinel 2	14 April 2021 15 May 2021	10	12 (16) *

4. Results

In this section, the results of annual and seasonal changes in the velocity and terminus position (Figures 2–4) of the Hornbreen–Hambergbreen system are presented. In addition, there is a discussion on how these change with environmental factors such as: air temperature, PDD, SST, total precipitation, and rainfall. All box plot contains standard statistical indicators (median, mean, min/max values, interquartile range), outliners are marked as dots (all values outside of interquartile range).

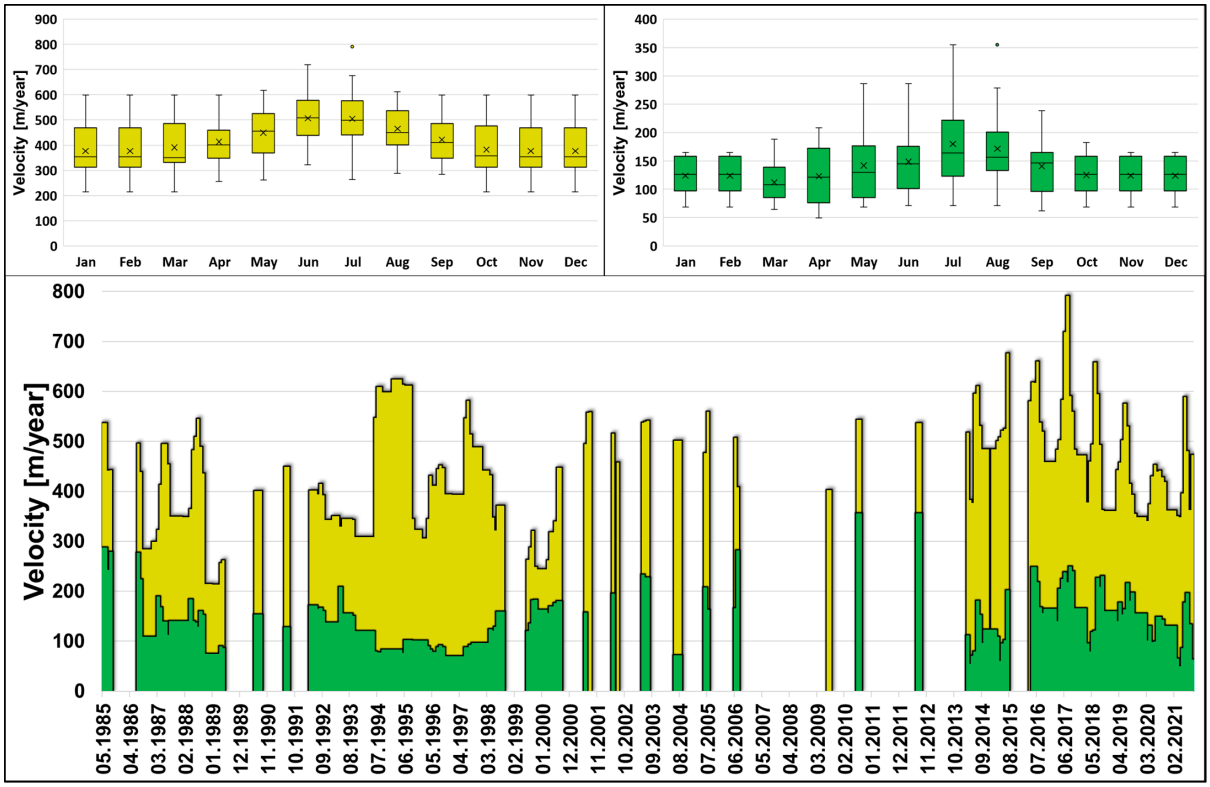

Figure 2. Seasonal and monthly velocities of Hornbreen (yellow) and Hambergbreen (green) in the 1985–2021 period.

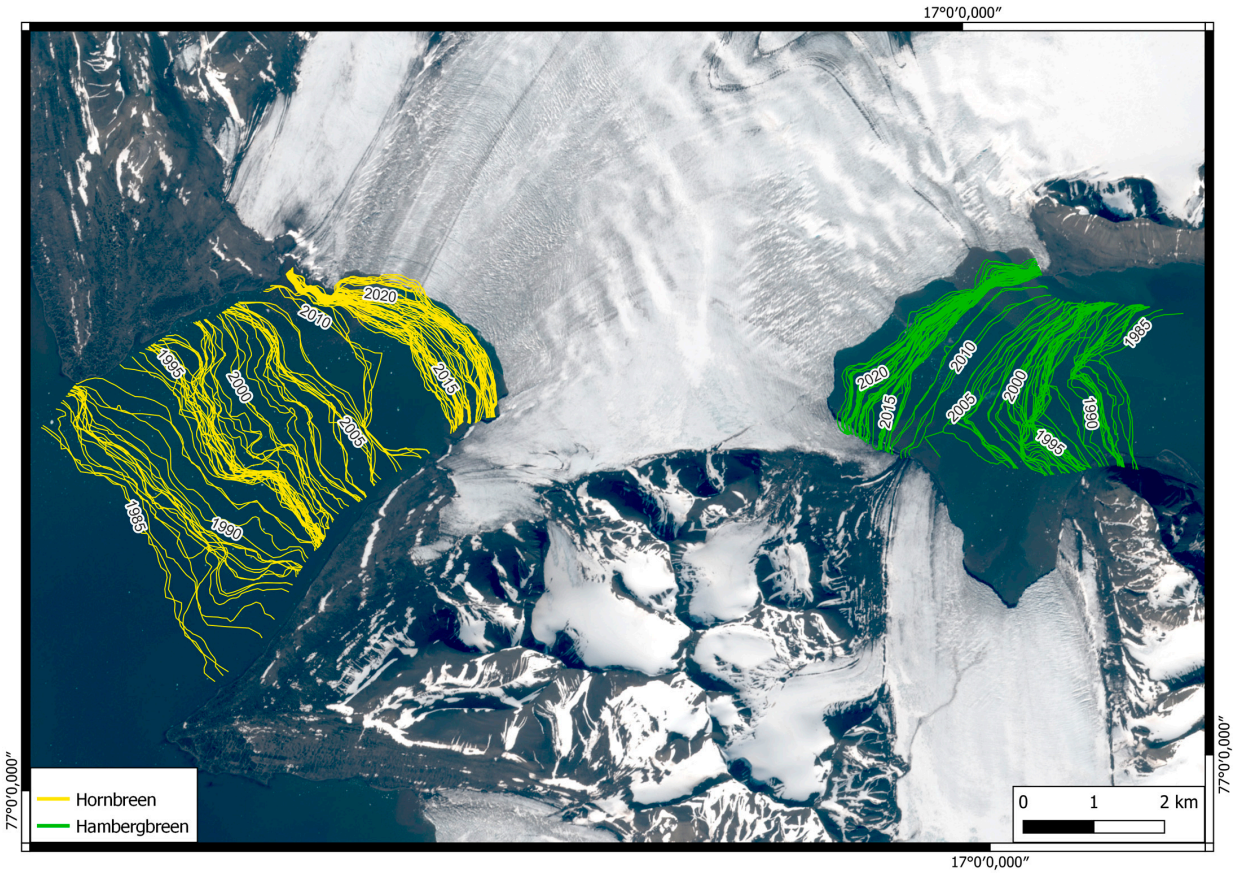

Figure 3. Termini positions of the HH system glaciers in the period 1985–2021.

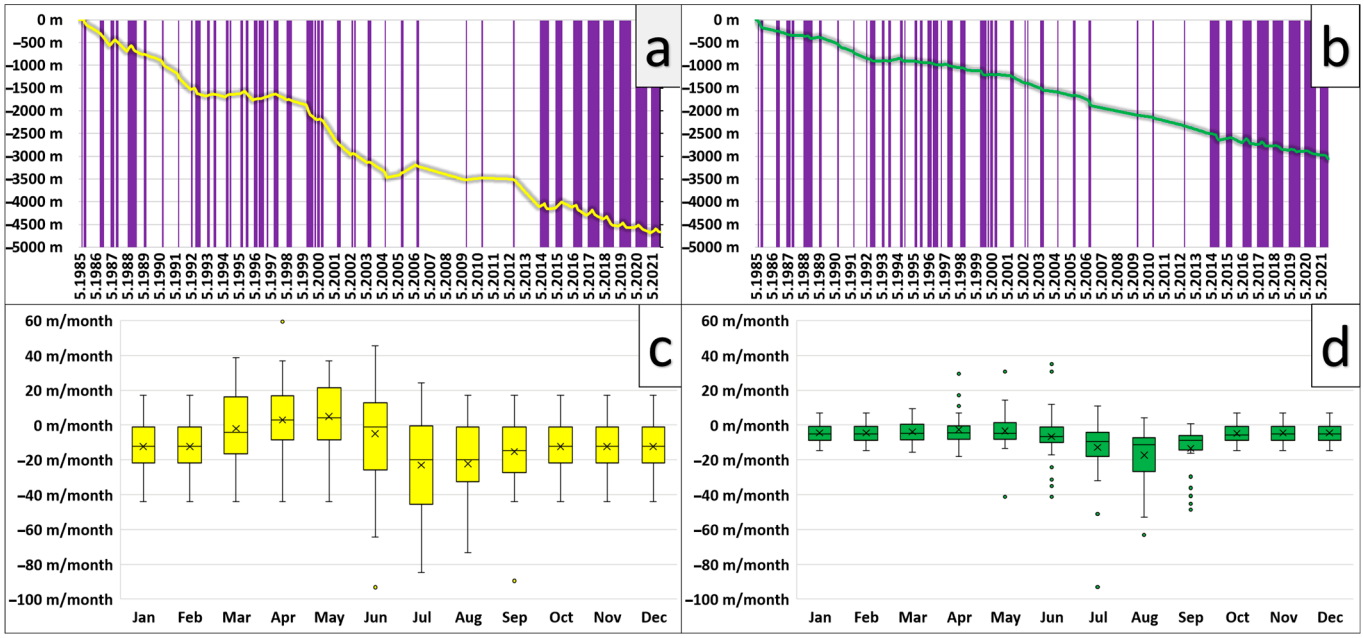

Figure 4. Seasonal (**c**,**d**) and cumulative (**a**,**b**) changes of the positions of the Hornbreen (**a**,**c**) and Hambergbreen (**b**,**d**) termini in the period 1985–2021. Observations are represented by purple stripes.

4.1. Hornbreen

The average annual Hornbreen velocity during the research period was 431 m a^{-1}. The maximum velocity value was recorded in July 2017 and reached 791 m a^{-1}, while the minimum in the 1988/1989 winter season was 214 m a^{-1}. The statistical trend of an increase in the velocity in Hornbreen amounted to 2.75 m a^{-1}/year in 1985–2021. An increase in velocity was also observed in each of the months investigated. The greatest increase was noted in June (4.4 m a^{-1}/year), and the smallest in November–February (1.4 m a^{-1}/year). It was estimated that the accuracy of the output velocities, based on the measurement of in situ ablation stakes, was 97%.

The velocity of Hornbreen increases at the end of spring, reaches a peak in June/July, and then slows down towards the winter (minimum seasonal velocities). In July, the velocity fluctuates the most, while in September, it is the most stable (Figure 2). For the years for which velocity data are available for all months, we recognised three types of glacier velocities: typical (peaks in the ablation season and lowest velocities in winter) [47–49], steady (the difference between maximum and minimum yearly velocities does not exceed 150 m a^{-1} for Hornbreen and 50 m a^{-1} for Hambergbreen), and abnormal (remaining cases). Only the data from1987 were slightly different from this pattern because the velocity peak was earlier in the season, in May/June. In 1993–1995, the glacier velocity showed a specific behaviour. In 1993, the amplitude of the velocity did not exceed 50 m a^{-1} (300–350 m a^{-1}); afterwards, in 1994, the glacier velocity doubled and reached 600 m a^{-1}. The glaciers also maintained this speed during the winter season, and the velocity decreased in September of 1995.

The glacier terminus retreated by 4.7 km during the research period (Figure 4). The mean rate of recession was 132 m a^{-1}. The lengthwise shrinking of the glacier was interrupted by episodes of advance or stagnation (1994–1995, 2004–2006). Rapid retreat was observed in 2000/2001 and 2012–2014. The glacier was advancing at the end of winter and spring, and the maximum extent was noted in April/May. Hornbreen began retreating with the start of the ablation season, reaching its maximum rate in July. The most rapid recession was recorded in June 1991, while the greatest rate of advance was in April 1988. The maximum variability of changes in terminus position occurred in July, and the minimum variability was recorded in the winter seasons.

4.2. Hambergbreen

The mean annual velocity of Hambergbreen in the study period was 141 m a^{-1}. The maximum speed occurred in July/August 2012 (355 m a^{-1}), while the minimum was in April 2021 (49 m a^{-1}). The Hambergbreen velocity tends to accelerate by 0.8 m a^{-1}/year. The fastest increase in velocity occurred in September (2.4 m a^{-1}/year), and the velocities tended to slow down in May–July, (down to 1.1 m a^{-1}/year in July); in the remaining months, velocities were increasing.

With the end of the polar night, the velocities continued to decline and reached a minimum in March and then they increased with a peak in July. Afterwards, velocity decreased to the winter values. The maximum variability of velocities occurred in July, while the minimum occurred during winter (Figure 2). Peaks in July/August were a feature of the "typical" style of velocities and were preceded by a decrease in speed after the polar night. The abnormal style of movement generally had two peaks of velocity, first in March/April and second in July/August (1993 was an exception without a second peak).

Hambergbreen retreated by 3.1 km during the research period (Figure 4), with a mean retreat rate of 84 m a^{-1}. There was one long episode of advance in 1992–1994. Short advances generally occurred in winter and early spring, and then, along with the start of the ablation season, the glacier shrank and reached a maximum recession rate in July. After this, it slowed down until it reached the winter rate. The highest recorded rate of retreat was in July 2006 (93 m/month), while the maximum advance was in June 2017.

4.3. Climatic and Oceanographic Conditions

4.3.1. Meteorological Conditions

PDD and air temperature tended to rise in the research period (Figure 5). Decadal temperature growth was 1.1 °C, and PDD tends to rise by 42.8 °C/decade. Both values are strongly correlated ($r = 0.79$, $p < 0.0001$). The maxima of average temperature and PDD occurred in 2016 and were 0.3 °C and 798.3 °C, respectively. The minimum values of the average annual air temperature and PDD occurred in 1988 (−7.2 °C and 310.4 °C, respectively). Two large increases in temperature were also noted in the short periods 1988–1990 and 2003–2006.

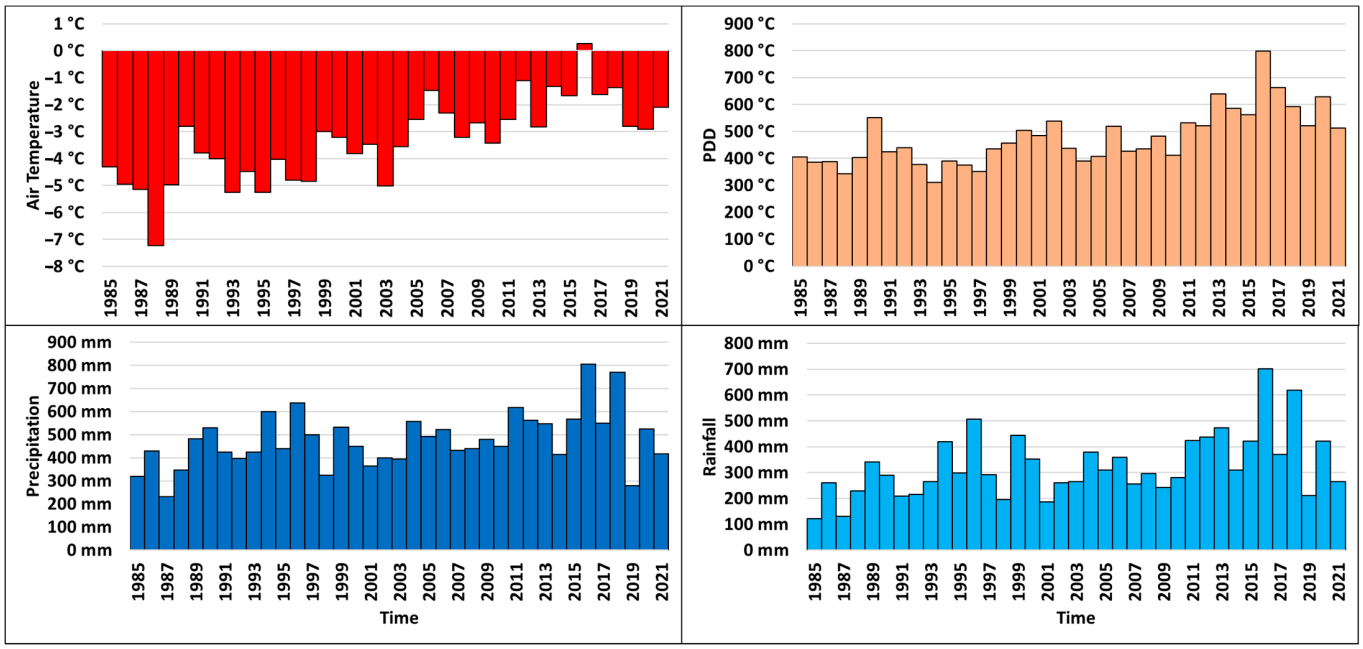

Figure 5. Annual air temperature (**top-left**), PDD (**top-right**), total precipitation (**bottom-left**), and rainfall (**bottom-right**).

The total precipitation and rainfall values were strongly correlated with each other (r = 0.93, $p < 0.0001$). Both parameters showed an upward trend of 5.5 mm/year for total precipitation and 4.4 mm/year for rainfall. The maxima of total precipitation and rainfall occurred in 2016 and amounted to 805.8 mm and 701.7 mm, respectively. The minimum value for total precipitation occurred in 1987 (230 mm) and for rainfall in 1985 (121.5 mm) (Figure 5).

The highest air temperature and PDD values were observed in July, while the lowest were in March. Temperatures in winter have a greater range than in summer; PDD shows the opposite pattern. The highest sums of total precipitation and rainfall occurred in August, while the lowest were in April. The range of monthly total precipitation increased along with its sum (Figure 6).

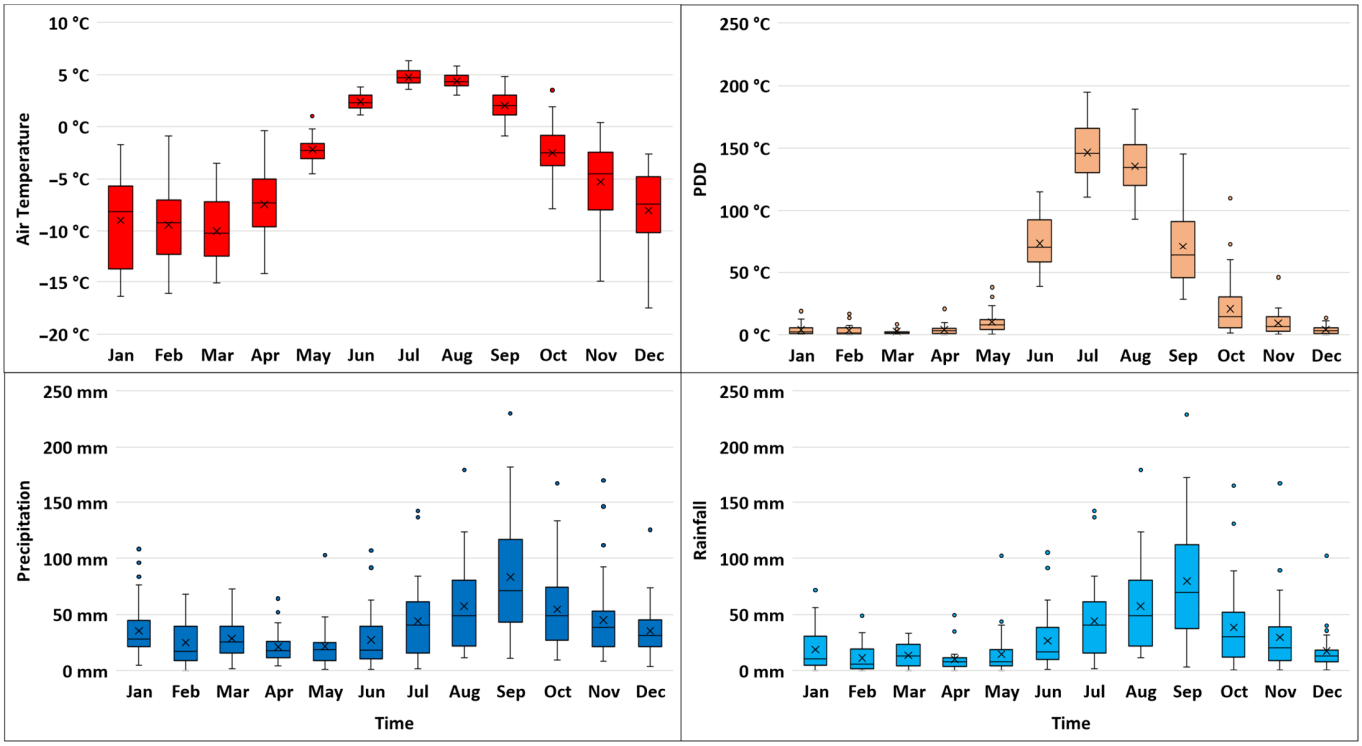

Figure 6. Seasonal air temperature (**top-left**), PDD (**top-right**), total precipitation (**bottom-left**), and rainfall (**bottom-right**).

4.3.2. Oceanographic Conditions

Mean annual SST near Hornbreen's ice cliff was 0.14 °C, while in front of Hambergbreen, it was 0.04 °C. Both temperatures were strongly correlated with each other (r = 0.81, $p < 0.0001$). SST showed a trend to increase, but it was more intense in the vicinity of Hambergbreen than in the vicinity of Hornbreen. Five periods of a fast rise in SST were observed in 1989/1990, 1997–2002, 2004–2006, 2011–2014, and 2016/2017. The SST in front of Hornbreen reached its maximum of 1.17 °C in 2018, while the minimum was in 1997 (−0.74 °C). In the case of Hambergbreen, the maximum was 1.48 °C in 2016, and the minimum −0.8 °C in 1996. The highest monthly SST values occurred in August, and the minima were typically in April (Figure 7).

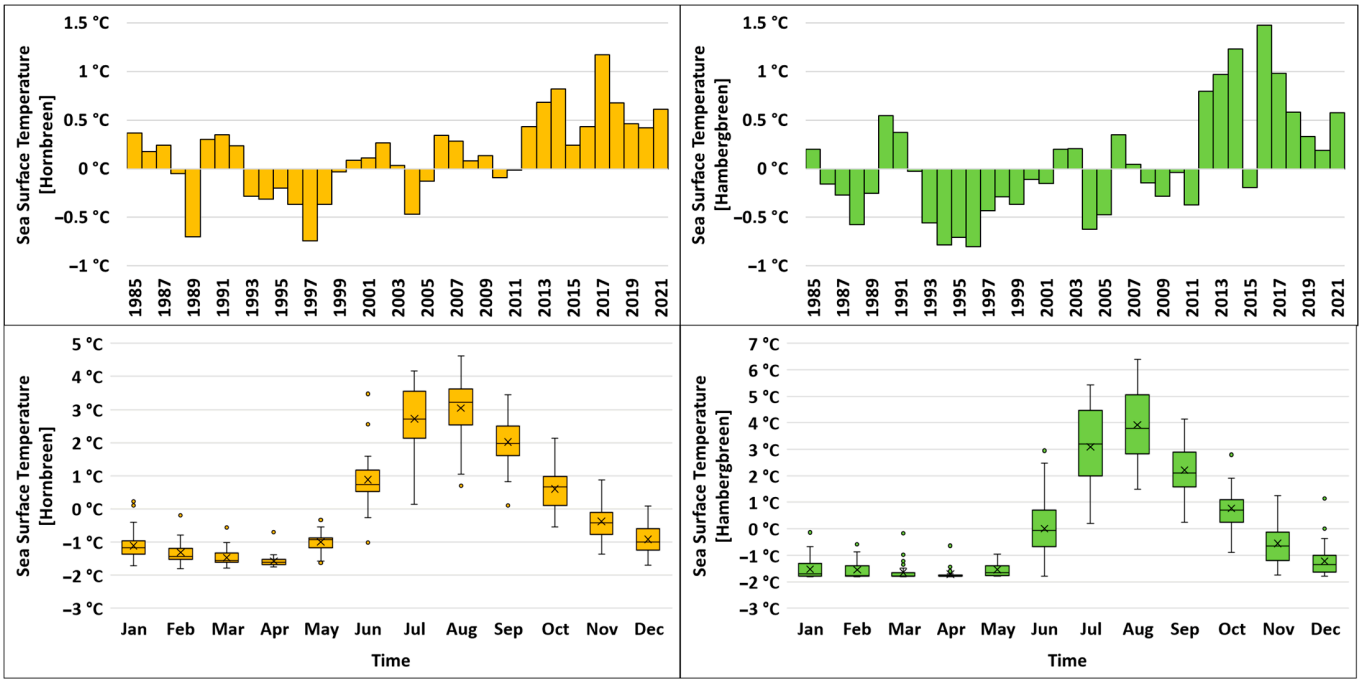

Figure 7. Annual and seasonal SST for Hornbreen (orange) and Hambergbreen (green).

4.4. Influence of Radiometric Resolution on the Quality of the Velocity Maps

A visual comparison of the velocity maps shows increased noise in the data based on an 8-bit pixel resolution (Figure 8). However, there is a significant difference between the data from Landsat 5 and ASTER, which may be due to the greater number of satellite images used to calculate velocity maps by the former (Table 1). Average annual velocities based on Landsat 5 data are of lower quality than those based on a 16-bit pixel depth; however, one can obtain the velocities in the upper part of the glacier (which is not the case in ASTER) (Figure 8). This indicates that the negative impact of low radiometric resolution can be reduced by using an increased number of images.

Figure 9 and Table 3 present the effect of changing pixel depth from 16 to 8 bit on the correctness of feature tracking-based velocity maps.

Table 3. Percentage share of pixels classified as one of 3 classes (correct values, noise, and no data) and the change between 16-bit and 8-bit resolution.

Class	L8 16-Bit Summer	L8 16-Bit Winter	L8 8-Bit Summer	L8 8-Bit Winter	S2 16-Bit Summer	S2 16-Bit Winter	S2 8-Bit Summer	S2 8-Bit Winter
Correct values	73.8	35.7	28.7	22.9	56.1	76.5	36.1	26.2
Noise	1.3	5.4	6.0	5.5	3.1	1.4	4.9	2.4
No Data cells	25.0	58.9	65.3	71.6	40.9	22.1	59.1	71.3
Correct values	Percentage difference between 16-bit- and 8-bit-based Landsat 8 velocity maps		−45.1	−12.7	Percentage difference between 16-bit- and 8-bit-based Sentinel 2 velocity maps		−20.0	−50.2
Noise			4.7	0.0			1.8	1.0
No Data cells			40.4	12.7			18.2	49.2

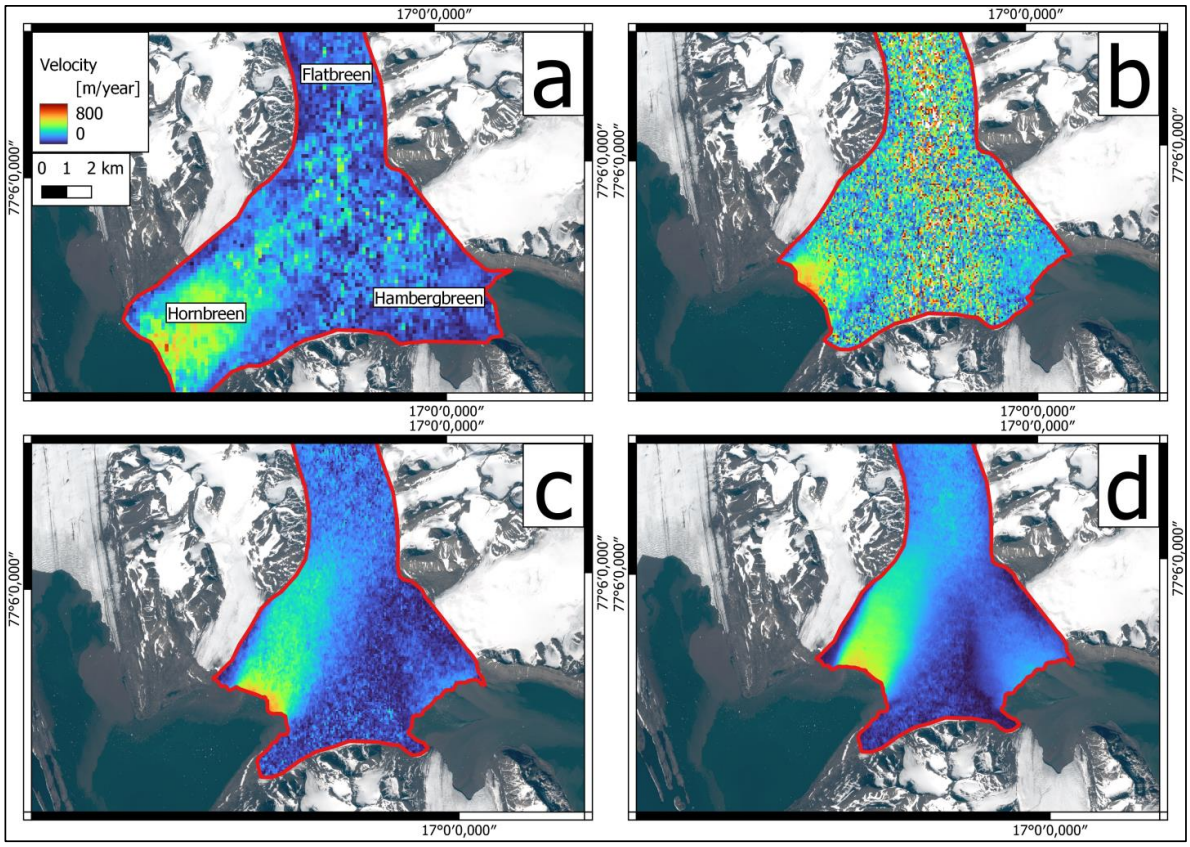

Figure 8. Mean velocities of the HH system based on data from different sensors (**a**) Landsat 5, (**b**) ASTER, (**c**) Landsat 8, and (**d**) Sentinel 2, for the periods specified in Table 1.

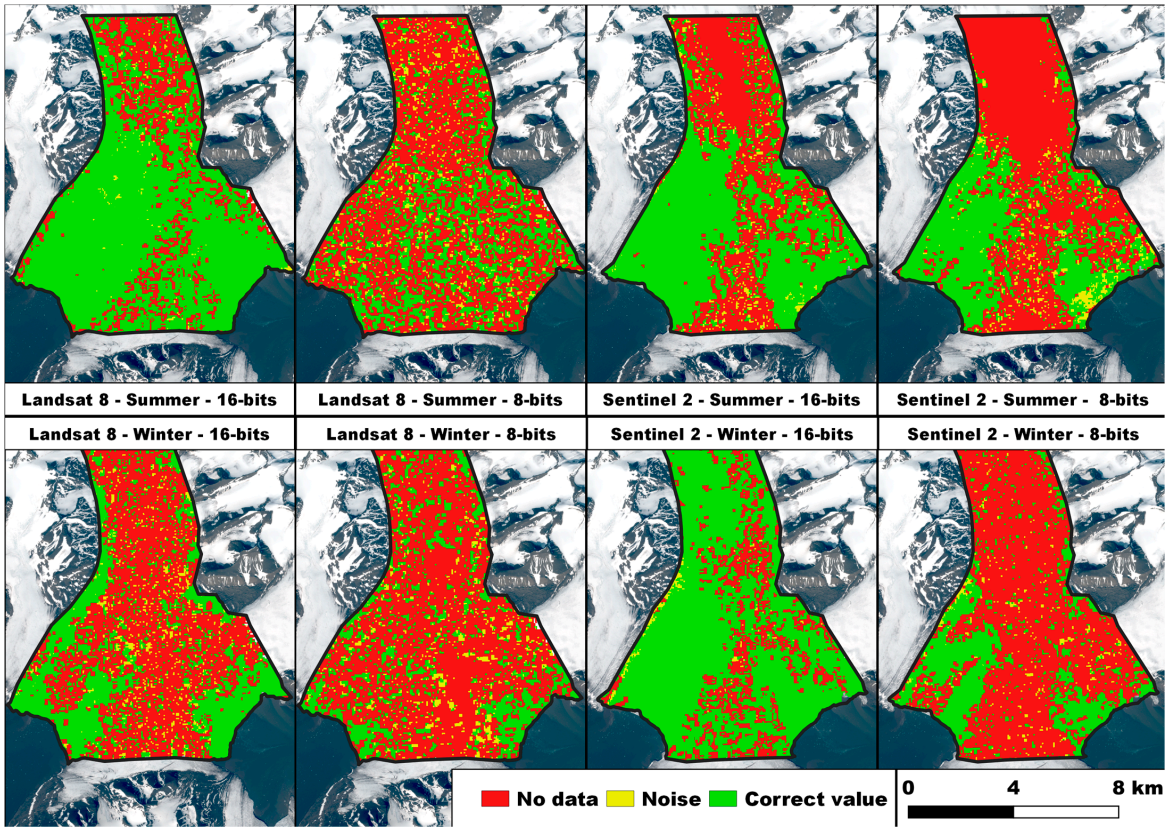

Figure 9. Comparison of velocity maps based on original and downgraded imagery.

A significant improvement in the quality of output data was noted in all cases (along with an increase in radiometric resolution). The increase in the proportion of correct cells varies (12.7–50.2%). No link was found with the presence of snow cover; in the case of Landsat 8, the increase in correct data was approximately 3 times higher in summer than in winter. However, in the case of Sentinel 2 data, the opposite relationship was found. Along with the improvement of correct values, a decrease was observed in noise and cells with no data. The decrease in noise cells was small and varied from 0% to 4.7% (Table 3). Along with improving the radiometric resolution of the image pairs, a significant decrease was found in the number of cells with no data. Their range varied in a manner similar to the cells with correct values. If the velocity maps based on 8- and 16-bit data are compared, it will be noted that the correct values appear, especially at the glacier terminus.

5. Discussion

Glaciological and climatic factors drive the difference between the annual velocities of the glaciers investigated. Hornbreen drains more ice masses than Hambergbreen [11] and at a greater extent. This enhances ice pressure near the terminus and explains differences in the velocities of the glaciers [47,50]. Hambergbreen is fed partly by Flatbreen, Skjoldfonna, and ice masses from the south slopes of the research area, while Hornbreen is fed by large ice masses from Flatbreen. Thus, the second glaciological factor explaining the slower movement of Hambergbreen is the contribution of slow-moving Skjlodfonna and inactive ice masses to the glacier ice flux. Velocity maps (Figure 8) show a faster ice stream in Hornbreen (than in Hambergbreen) all along the centrelines. This indicates that glaciological factors (extent, arrangement of tributaries) play a primary role in conditioning glacier velocities. The differences in sea temperature between the east and west coast caused by sea currents can be recognised as a secondary factor influencing the velocities of the HH system. Air temperature is connected to SST [32], and a statistically significant (p = 0.001) correlation is found between mean monthly air and sea surface temperatures near Hornbreen and Hambergbreen ice cliffs (Hornbreen, r = 0.83; Hambergbreen, r = 0.78). Higher temperatures on the west side of the HH system [31,51] intensify the melting of the glacier surface and the supply of freshwater to the glacial system [44]. Both glaciers tend to increase velocity, and this is a common behaviour of Svalbard glaciers [4]. These changes can be linked to very high (1.14 °C/decade) rising air temperatures, which cause intense melting and a decrease in the area of Firn in the accumulation zone [24], which retains water. Both of these factors led to an increase in the water supply to the glacial system in the study period. More water in glacial systems raises subglacial water pressure, which could cause an acceleration of the glacier [47,52,53].

Monthly maximum and minimum velocities are delayed by approximately one month on Hambergbreen in comparison to Hornbreen (Figure 4). This could be caused by the faster development of the hydroglacial system on the west side of the research area caused by higher air temperatures. Increases in seasonal glacier velocity depend mainly on water supply [52,53] caused by intense melting or rainfall. The velocities of both glaciers decrease in late summer/early autumn despite high temperatures and rainfall. These phenomena are explained by the fact that an increase in subglacial water pressure can only occur if an extensive network of conducted channels exists. Along with the duration of the ablation season, the hydrological network evolves into an efficient, channelised drainage system. That kind of drainage can efficiently expel water and prevent the increase in subglacial water pressure. This behaviour is also described for other Svalbard glaciers [14,54,55]. In Hambergbreen, speed-up events in late winter/early spring are often noted. Similar events were observed on nearby Hansbreen [56] and were caused by winter thaws and rainfalls [2,29].

To explain the long-term increase in glacier velocity, correlations were made between mean annual and monthly velocity data (in the years when all monthly data were collected) and air temperature, SST, PDD, total precipitation, and rainfall. (Table 4). A very strong correlation was found between annual Hambergbreen velocities and SST/PDD. An aver-

age/low correlation was also found between all monthly velocities and thermal factors (air temperature, SST, PDD) as well as no/low correlation with total precipitation.

Table 4. Correlations between glacier velocities and selected environmental factors (statistically important results are highlighted).

	Glacier	SST	Tair	PDD	Precipitation	Rainfall
All monthly values	Hambergbreen	0.41 $p < 0.0001$	0.31 $p < 0.0001$	0.37 $p < 0.0001$	0 $p = 0.999$	0.06 $p = 0.431$
	Hornbreen	0.32 $p < 0.0001$	0.41 $p < 0.0001$	0.4 $p < 0.0001$	0.1 $p = 0.159$	0.16 $p < 0.0001$
Annual (in years with data for all months)	Hambergbreen	0.85 $p < 0.0001$	0.54 $p = 0.087$	0.73 $p < 0.0001$	−0.15 $p = 0.668$	−0.09 $p = 0.797$
	Hornbreen	0.3 $p = 0.378$	0.43 $p = 0.187$	0.31 $p = 0.353$	0.36 $p = 0.276$	0.27 $p = 0.425$

Next three styles of glacier velocity were correlated with environmental factors (Table 5). The typical style of velocity seen in Hambergbreen showed a high correlation with all thermal factors and a lack of correlation with total precipitation. The steady and abnormal styles showed no link with environmental factors. The high correlation of SST (also annual) with velocity suggests an indirect link between these factors. Higher SST values influence the enhancing of the calving rate and glacier terminus recession. This leads to a weakening of the glacier grounding, surface stretching, and acceleration of velocity [57–61]. An additional explanation of the SST and velocity link could show a high correlation between air temperatures and SST, suggesting that an increased velocity is a consequence of increased melting caused by higher temperatures. A slightly different style of relationship between velocities and environmental factors was found for Hornbreen. The glacier showed medium/high correlations between thermal factors and all styles of motion distribution. A low correlation was also found between the typical style and total precipitation and a medium correlation between steady style and rainfall. This suggests that rainfall contributes to the subglacial water level and plays a secondary role in forcing glacier velocity (visible only in particular circumstances, e.g., steady velocity) [47,52,53].

Table 5. Correlations between monthly velocities of yearly velocity styles and selected environmental factors (statistically significant results are highlighted).

Glacier	Type of Velocity	SST	Tair	PDD	Precipitation	Rainfall
Hambergbreen	Typical	0.65 $p < 0.0001$	0.61 $p < 0.0001$	0.62 $p < 0.0001$	0.23 $p = 0.179$	0.25 $p = 0.184$
	Steady	0.02 $p = 0.871$	0.02 $p = 0.899$	−0.06 $p = 0.716$	−0.05 $p = 0.738$	−0.21 $p = 0.208$
	Abnormal	0.10 $p = 0.488$	0.12 $p = 0.404$	−0.04 $p = 0.838$	0.01 $p = 0.951$	−0.14 $p = 0.399$
Hornbreen	Typical	0.49 $p < 0.0001$	0.68 $p < 0.0001$	0.54 $p < 0.0001$	0.26 $p = 0.046$	0.23 $p = 0.121$
	Steady	0.53 $p = 0.001$	0.57 $p < 0.0001$	0.51 $p = 0.004$	0.27 $p = 0.112$	0.42 $p = 0.023$
	Abnormal	0.34 $p = 0.040$	0.33 $p = 0.048$	0.46 $p = 0.013$	0.10 $p = 0.547$	0.21 $p = 0.286$

The annual average retreat rate for Hornbreen was 128 m a^{-1}, while for Hambergbreen, it was 84 m a^{-1}. A medium correlation was found between the fluctuations of the

Hornbreen terminus and SST/PDD. Other factors show low or no correlation. In the case of Hambergbreen, a medium correlation was found between its changes in extent and air temperature/SST as well as with rainfall (low correlation). Based on an analysis of the location of the termini of both glaciers, a faster rate of retreat for Hornbreen is the consequence of higher values of SST on the west side of the research area. Annual SST and velocity provide a good explanation for the position of the termini (with exceptions).

Seasonal fluctuations of the termini of the HH system vary in time. Despite the lack of a minimum position of the terminus due to the lack of optical images during the polar night, the features of glacier retreat were determined from late summer data. The fluctuation interval of the extent of Hambergbreen is mainly determined by outliers, and is shorter than in the case of Hornbreen. Advances in late winter/early spring were evident in the case of Hornbreen. The reason for the advance in this period is provided by the low SST values that decrease calving activity [62] and velocities. During the ablation season, the glacier termini retreat due to rising values of SST and an intensification of the water circulation in front of the ice cliffs. These factors further enhance glacier calving activity [63]. The development of an efficient subglacial system, which slows down the glacier and intense calving, leads to maximum retreat rate values in the middle of the ablation season. Then, with the decrease in air and sea temperatures, the glacier retreat rate slows and stagnates. In September, massive recession episodes of the Hambergbreen terminus were noted, which can be linked to the highest rainfall occurring in this month. Rainfall can increase calving activity by filling crevasses near the termini with water [64]. The minimum and maximum values of the changes in extent were obtained about one month later on Hambergbreen (when compared to Hornbreen)—in a similar manner to velocity.

Finally, the date of the opening of the fiord was estimated on the basis of more updated and frequent data than those used by previous authors. Results were convergent (31 years—Hornbreen, 32 years—Hambergbreen). This leads to the conclusion that the Hornsund strait will be open again in ~2053. Our calculations are very simple and do not predict any surges, and the date of the disintegration of the HH system is based only on the mean recession rate. Ziaja and Ostafin concluded that the strait will be open in 2030–2035 [9]. However, their calculations are based on the distance between the termini of both glaciers and do not include subglacial relief. Thus, the predictions are too rapid. In contrast, Grabiec and others suggest the 2055–2065 period [11], which is slightly later than our estimate. This could result from the use of the latest data for the prediction in this paper.

Our secondary task, an assessment of the importance of the influence of radiometric resolution on output velocity maps, shows a general improvement in data quality along with a greater pixel depth. Low spatial resolution imagery (Landsat 5, Landsat 7, ASTER) is characterised by a significant presence of noise and 'no data' cells, especially in the upper parts of the glaciers investigated. In the velocity maps based on data from Landsat 8 and Sentinel 2, the disruptions are very limited. However, Landsat 5-based maps are much more artefact-free than ASTER. This suggests that a negative impact of a lower radiometric resolution can be overcome by the increased use of satellite imagery pairs used for velocity estimation.

The reclassified velocity maps were also quantified on the basis of the dataset cited in Table 3. In 8-bit-based velocity maps, the majority of cells were recognised as no data, and along with improving the pixel depth to 16 bits, their percentage share decreased in favour of the correct values. There was only a small (0–4.7%) decrease in noise. In general, more 'no data' cells were recognised than noise ones; this disproportion varies between 10 to 30 times. This leads to the conclusion that the increase in correct cells is a consequence of a better ability to recognise surface features linked to a greater pixel depth. Research on the impact of radiometric resolution is mainly focused on the possibility of the proper recognition of land features (crevasses, etc.). Problems in this field are conditioned by an increased saturation in shadowed regions. A greater pixel depth reduces this phenomenon and allows the feature tracking algorithm to define unique surface features [21,65]. Another idea could be a better ability to recognise snow facies by imagery with better radiometric

resolution [22]. Varied snow cover conditions (e.g., percolation, snowdrifts on the glacier surface, deposits of darker materials) could also be interpreted as surface features.

6. Conclusions

This paper has analysed the velocities and fluctuations of the termini of two tidewater glaciers, Hornbreen and Hambergbreen, in 1985–2021. Analyses were conducted using remote sensing (optical imagery, SST) data and in situ measurements (air temperature, precipitation, ablation stakes). It was concluded that:

- An increased quality of output velocity maps is caused by an improved ability to recognise surface features, connected to the improved radiometric resolution of optical imagery.
- An improvement in the quality of velocity maps (between 8-bit- and 16-bit-based maps) varied from 12.5% to 50.2%. No link was found between the level of improvement and the presence of snow cover.
- The mean velocity of Hornbreen was 431 m a^{-1} and that of Hambergbreen was 141 m a^{-1}. The difference in velocities depends mainly on the glaciological characteristics, such as glacier extent, and the complexity of the direction of ice flow near the terminus (e.g., tributary ice flow from Skjoldfonna); the influence of climatological conditions on glacier velocity was of secondary importance.
- Both glaciers accelerated in the study period: Hornbreen on average by 2.75 m/year and Hambergbreen on average by 0.8 m/year. The cause could be an increase in the water supply to the drainage system due to surface melting caused by an increase in air temperature (1.14 °C/decade).
- Maximum and minimum monthly values of velocities and fluctuations of the termini are about one month later in Hambergbreen than in Hornbreen; the reason for this behaviour could be a faster evolution of the drainage system and higher temperatures on the west side of the HH system.
- Thermal factors are primary climatic components that condition the velocities and changes in the positions of termini (an increased role of SST in the case of the velocity of Hambergbreen), while rainfall is the secondary component that influences glacier behaviour in particular circumstances.
- Both glaciers retreated in the study period, Hornbreen by 4.7 km and Hambergbreen by 3.1 km. The reason for the difference is the different velocities of the glaciers and the higher values of thermal factors, which enhance calving activity, as well as topography.
- If recession continues at the current rate, the Hornsund strait will reopen in ~2053.

Author Contributions: Conceptualisation, D.S., M.B. and B.G.; methodology, D.S., M.B. and M.G.; software, D.S.; validation, D.S. and M.B.; data curator, D.S.; writing—preparation of original draft, D.S.; writing—review and editing, M.B., M.G. and B.G. All authors have read and agreed to the published version of the manuscript.

Funding: This research received no external funding.

Data Availability Statement: The satellite imagery used in this study was obtained from EarthExplorer, a platform provided by the United States Geological Survey (USGS). CTD and ablation stakes data were collected during Polish–Norwegian AWAKE (PNRF-22-AI-1/07) and AWAKE-2 (Pol-Nor grant 198675/17/2013), projects. Data are available at individual databases: SST—https://doi.org/10.24381/cds.cf608234 (accessed on 6 July 2023); CTD—https://odis.iopan.pl/AWAKE/ (accessed on 6 July 2023); ablation stakes—https://ppdb.us.edu.pl:/geonetwork/srv/api/records/37a59a98-835f-4f98-ab39-52c8d9cb7290 (accessed on 6 July 2023).

Acknowledgments: The authors express their gratitude to Jacek Jania and the participants of the polar expedition of the University of Silesia in Katowice 2021 for their valuable assistance during the fieldwork. Additionally, the authors extend their thanks to the staff of the Institute of Geophysics PAS and the Polish Polar Station, Hornsund, for their support and assistance throughout the field campaign. The research and logistic equipment of the Polar Laboratory of the University of Silesia in Katowice was used during the fieldwork. We would like to thank the three anonymous reviewers who provided very thoughtful and constructive feedback that helped improve the paper.

Conflicts of Interest: The authors declare no conflict of interest.

References

1. AMAP. *Arctic Climate Change Update 2021: Key Trends and Impacts—Summary for Policy-Makers*; Arctic Monitoring an Assessment Programme (AMAP): Tromsø, Norway, 2021.
2. Wawrzyniak, T.; Osuch, M. A 40-Year High Arctic Climatological Dataset of the Polish Polar Station Hornsund (SW Spitsbergen, Svalbard). *Earth Syst. Sci. Data* **2020**, *12*, 805–815. [CrossRef]
3. Błaszczyk, M.; Jania, J.A.; Kolondra, L. Fluctuations of tidewater glaciers in Hornsund Fjord (Southern Svalbard) since the beginning of the 20th century. *Pol. Polar Res.* **2013**, *34*, 321–352. [CrossRef]
4. Strozzi, T.; Paul, F.; Wiesmann, A.; Schellenberger, T.; Kääb, A. Circum-Arctic Changes in the Flow of Glaciers and Ice Caps from Satellite SAR Data between the 1990s and 2017. *Remote Sens.* **2017**, *9*, 947. [CrossRef]
5. Ziaja, W.; Ostafin, K. Origin and Location of New Arctic Islands and Straits Due to Glacial Recession. *Ambio* **2019**, *48*, 25–34. [CrossRef] [PubMed]
6. Szupryczyński, J. *(1934-) Prace Geograficzne/Instytut Geografii Polskiej Akademii Nauk*; nr 71. CBGiOŚ. IGiPZ PAN Call No. 29.103; Państwowe Wydawnictwo Naukowe: Warszawa, Poland, 1968.
7. Koryakin, V.S. The Position and Morphology of Glaciers. In *Glaciation of Spitsbergen (Svalbard)*; Troitsky, L.S., Singer, E.M., Koryakin, V.S., Markin, V.A., Mikhaliov, V.I., Eds.; Nauka: Moscov, Russia, 1975; pp. 7–41.
8. Sharov, A.; Osokin, S. Controlled Interferometric Modelling of Glacier Changes in South Svalbard. *Fringe 2005 Workshop* **2006**, *610*, 27.
9. Ziaja, W.; Ostafin, K. Landscape–Seascape Dynamics in the Isthmus between Sørkapp Land and the Rest of Spitsbergen: Will a New Big Arctic Island Form? *AMBIO* **2015**, *44*, 332–342. [CrossRef]
10. Pälli, A.; Moore, J.; Jania, J.; Glowacki, P. Glacier Changes in Southern Spitsbergen, Svalbard, 1901-2000: International Symposium on Physical and Mechanical Processes Om Ice in Relation to Glacier and Ice-Sheet Modelling. *Ann. Glaciol.* **2003**, *37*, 219–225. [CrossRef]
11. Grabiec, M.; Ignatiuk, D.; Jania, J.; Moskalik, M.; Głowacki, P.; Błaszczyk, M.; Budzik, T.; Walczowski, W. Coast Formation in an Arctic Area Due to Glacier Surge and Retreat: The Hornbreen–Hambergbreen Case from Spistbergen. *Earth Surf. Process. Landf.* **2018**, *43*, 387–400. [CrossRef]
12. Kavan, J.; Tallentire, G.D.; Demidionov, M.; Dudek, J.; Strzelecki, M.C. Fifty Years of Tidewater Glacier Surface Elevation and Retreat Dynamics along the South-East Coast of Spitsbergen (Svalbard Archipelago). *Remote Sens.* **2022**, *14*, 354. [CrossRef]
13. Błaszczyk, M.; Moskalik, M.; Grabiec, M.; Jania, J.; Walczowski, W.; Wawrzyniak, T.; Strzelewicz, A.; Malnes, E.; Lauknes, T.R.; Pfeffer, W. The Response of Tidewater Glacier Termini Positions in Hornsund (Svalbard) to Climate Forcing, 1992–2020. *J. Geophys. Res. Earth Surf.* **2023**, *128*, e2022JF006911. [CrossRef]
14. Błaszczyk, M.; Jania, J.A.; Ciepły, M.; Grabiec, M.; Ignatiuk, D.; Kolondra, L.; Kruss, A.; Luks, B.; Moskalik, M.; Pastusiak, T.; et al. Factors Controlling Terminus Position of Hansbreen, a Tidewater Glacier in Svalbard. *J. Geophys. Res. Earth Surf.* **2021**, *126*, e2020JF005763. [CrossRef]
15. Scambos, T.A.; Dutkiewicz, M.J.; Wilson, J.C.; Bindschadler, R.A. Application of Image Cross-Correlation to the Measurement of Glacier Velocity Using Satellite Image Data. *Remote Sens. Environ.* **1992**, *42*, 177–186. [CrossRef]
16. Bindschadler, R.A.; Scambos, T.A. Satellite-Image-Derived Velocity Field of an Antarctic Ice Stream. *Science* **1991**, *252*, 242–246. [CrossRef]
17. Gardner, A.S.; Moholdt, G.; Scambos, T.; Fahnstock, M.; Ligtenberg, S.; van den Broeke, M.; Nilsson, J. Increased West Antarctic and Unchanged East Antarctic Ice Discharge over the Last 7 Years. *Cryosphere* **2018**, *12*, 521–547. [CrossRef]
18. Friedl, P.; Seehaus, T.; Braun, M. RETREAT: A new freely available data set of Sentinel-1 glacier velocities in regions outside the polar ice sheets. In Proceedings of the EGU General Assembly 2021, Online, 19–30 April 2021; EGU21-2740. [CrossRef]
19. Van Wyk de Vries, M.; Wickert, A.D. Glacier Image Velocimetry: An Open-Source Toolbox for Easy and Rapid Calculation of High-Resolution Glacier Velocity Fields. *Cryosphere* **2021**, *15*, 2115–2132. [CrossRef]
20. Pellikka, P.; Rees, W.G. *Remote Sensing of Glaciers: Techniques for Topographic, Spatial and Thematic Mapping of Glaciers*; CRC Press: Boca Raton, FL, USA, 2009; ISBN 978-0-203-85130-2.
21. Kääb, A.; Winsvold, S.H.; Altena, B.; Nuth, C.; Nagler, T.; Wuite, J. Glacier Remote Sensing Using Sentinel-2. Part I: Radiometric and Geometric Performance, and Application to Ice Velocity. *Remote Sens.* **2016**, *8*, 598. [CrossRef]
22. Yousuf, B.; Shukla, A.; Arora, M.K.; Jasrotia, A.S. Glacier Facies Characterization Using Optical Satellite Data: Impacts of Radiometric Resolution, Seasonality, and Surface Morphology. *Prog. Phys. Geogr. Earth Environ.* **2019**, *43*, 473–495. [CrossRef]
23. Dallmann, W.K. *Geoscience Atlas of Svalbard*; Norsk Polarinstitutt: Tromsø, Norway, 2015; ISBN 978-82-7666-312-9.
24. Barzycka, B.; Grabiec, M.; Błaszczyk, M.; Ignatiuk, D.; Laska, M.; Hagen, J.O.; Jania, J. Changes of Glacier Facies on Hornsund Glaciers (Svalbard) during the Decade 2007–2017. *Remote Sens. Environ.* **2020**, *251*, 112060. [CrossRef]
25. Błaszczyk, M.; Hagen, J.O.; Jania, J.A. Tidewater Glaciers of Svalbard: Recent Changes and Estimates of Calving Fluxes. *Pol. Polar Res.* **2009**, *30*, 85–142.
26. Lefauconnier, B.; Hagen, J.O. *Surging and Calving Glaciers in Eastern Svalbard*; Norsk Polarinstitutt: Tromsø, Norway, 1991; ISBN 978-82-90307-94-8.

27. Peel, M.C.; Finlayson, B.L.; McMahon, T.A. Updated World Map of the Köppen-Geiger Climate Classification. *Hydrol. Earth Syst. Sci.* **2007**, *11*, 1633–1644. [CrossRef]
28. Perchaluk, J.; Szczurtek, S.; Ostrowski, P.; Flak, W.; Nowosad, P.; Ulandowska-Monarcha, P. Biuletyn Meteorologiczny—Podsumowanie Roku 2021, Spitsbergen—Hornsund. 2022. Available online: https://igfedupl-my.sharepoint.com/personal/dbartniak_igf_edu_pl/_layouts/15/onedrive.aspx?ga=1&id=%2Fpersonal%2Fdbartniak%5Figf%5Fedu%5Fpl%2FDocuments%2FBiuletyny%2FBIULETYN%5F44%2FReport%5F2021%5F0%2Epdf&parent=%2Fpersonal%2Fdbartniak%5Figf%5Fedu%5Fpl%2FDocuments%2FBiuletyny%2FBIULETYN%5F44 (accessed on 7 July 2023).
29. Matuszko, D.; Soroka, J. Charakterystyka odwilży w Hornsundzie (Spitsbergen). *Probl. Klimatol. Polarn.* **2016**, *26*, 59–70.
30. Marsz, A.A.R.; Styszyńska, A.R. *Climate and Climate Change at Hornsund, Svalbard*; Gdynia Maritime University: Gdynia, Poland, 2013.
31. Sulikowska, A.; Wypych, A.; Mitka, K.; Maciejowski, W.; Ostafin, K.; Ziaja, W. Summer weather conditions in 2005 and 2016 on the western and eastern coasts of south Spitsbergen. *Pol. Polar Res.* **2018**, *39*, 127–144.
32. Walczowski, W.; Piechura, J. Influence of the West Spitsbergen Current on the Local Climate. *Int. J. Climatol.* **2011**, *31*, 1088–1093. [CrossRef]
33. Asbjørnsen, H.; Årthun, M.; Skagseth, Ø.; Eldevik, T. Mechanisms Underlying Recent Arctic Atlantification. *Geophys. Res. Lett.* **2020**, *47*, e2020GL088036. [CrossRef]
34. Merchant, C.J.; Embury, O.; Bulgin, C.E.; Block, T.; Corlett, G.K.; Fiedler, E.; Good, S.A.; Mittaz, J.; Rayner, N.A.; Berry, D.; et al. Satellite-Based Time-Series of Sea-Surface Temperature since 1981 for Climate Applications. *Sci Data* **2019**, *6*, 223. [CrossRef]
35. Embury, O. Product Quality Assurance Document. Available online: https://datastore.copernicus-climate.eu/documents/satellite-sea-surface-temperature/v2.1/D2.SST.1-v3.0_PQAD_of_v2.1SST_products_v6.0_APPROVED_Ver1.pdf (accessed on 31 March 2022).
36. Fiedler, E.K.; Mao, C.; Good, S.A.; Waters, J.; Martin, M.J. Improvements to Feature Resolution in the OSTIA Sea Surface Temperature Analysis Using the NEMOVAR Assimilation Scheme. *Q. J. R. Meteorol. Soc.* **2019**, *145*, 3609–3625. [CrossRef]
37. Good, S.; Fiedler, E.; Mao, C.; Martin, M.J.; Maycock, A.; Reid, R.; Roberts-Jones, J.; Searle, T.; Waters, J.; While, J.; et al. The Current Configuration of the OSTIA System for Operational Production of Foundation Sea Surface Temperature and Ice Concentration Analyses. *Remote Sens.* **2020**, *12*, 720. [CrossRef]
38. ODIS-AWAKE. Available online: https://odis.iopan.pl/AWAKE/ (accessed on 6 July 2023).
39. Wawrzyniak, T.; Osuch, M. A Consistent High Arctic Climatological Dataset (1979–2018) of the Polish Polar Station Hornsund (SW Spitsbergen, Svalbard). 2019. Available online: https://doi.pangaea.de/10.1594/PANGAEA.909042 (accessed on 31 March 2022).
40. Available online: https://hornsund.igf.edu.pl/Biuletyny/ (accessed on 31 March 2022).
41. Sikora, S.; Migała, K.; Budzik, T.; Głowacki, P.; Puczko, D.; Ignatiuk, D.; Jania, J. System gromadzenia danych meteorologicznych i glacjologicznych w obszarach polarnych—infrastruktura pomiarowa polskiej stacji polarnej im. Stanisława Siedleckiego (SW Spitsbergen). *Przegląd Geofiz.* **2012**, *1*, 35–47.
42. Budzik, T. Air Temperature—Flatbreen. Available online: https://ppdb.us.edu.pl:/geonetwork/srv/api/records/eaa9217c-6bcf-4a35-bbda-bde3d879ee5d (accessed on 31 March 2022).
43. Fitch, A.J.; Kadyrov, A.; Christmas, W.J.; Kittler, J. Orientation Correlation. In Proceedings of the British Machine Vision Conference 2002; British Machine Vision Association: Cardiff, UK, 2002; pp. 11.1–11.10.
44. Błaszczyk, M.; Ignatiuk, D.; Uszczyk, A.; Cielecka-Nowak, K.; Grabiec, M.; Jania, J.A.; Moskalik, M.; Walczowski, W. Freshwater Input to the Arctic Fjord Hornsund (Svalbard). *Polar Res.* **2019**, *38*, 3506. [CrossRef]
45. Front Velocity of Tidewater Glaciers in Hornsund. Available online: https://ppdb.us.edu.pl:/geonetwork/srv/api/records/37a59a98-835f-4f98-ab39-52c8d9cb7290 (accessed on 6 July 2023).
46. Urbanski, J.A. A GIS Tool for Two-Dimensional Glacier-Terminus Change Tracking. *Comput. Geosci.* **2018**, *111*, 97–104. [CrossRef]
47. Benn, D.I.; Evans, D.J.A. *Glaciers & Glaciation*; Hodder Education: London, UK, 2010; ISBN 978-0-340-90579-1.
48. Iken, A. Velocity Fluctuations of an Arctic Valley Glacier: A Study of the White Glacier, Axel Heiberg Island, Canadian Arctic Archipelago [Jacobsen-McGill Arctic research expedition 1959–1962]. *Glaciology* **1974**, 5. [CrossRef]
49. Willis, I.C. Intra-Annual Variations in Glacier Motion: A Review. *Prog. Phys. Geogr. Earth Environ.* **1995**, *19*, 61–106. [CrossRef]
50. Cuffey, K.M.; Paterson, W.S.B. *The Physics of Glaciers*; Academic Press: Cambridge, MA, USA, 2010; ISBN 978-0-08-091912-6.
51. Maciejowski, W.; Michniewski, A.; Maciejowski, W.; Michniewski, A. Variations in Weather on the East and West Coasts of South Spitsbergen, Svalbard. *Pol. Polar Res.* **2007**, *2*, 123–136.
52. Iken, A.; Bindschadler, R.A. Combined Measurements of Subglacial Water Pressure and Surface Velocity of Findelengletscher, Switzerland: Conclusions about Drainage System and Sliding Mechanism. *J. Glaciol.* **1986**, *32*, 101–119. [CrossRef]
53. Jania, J. *Glacjologia: Nauka o Lodowcach*; Naukowe PWN: Warsaw, Poland, 1997; ISBN 978-83-01-12264-5.
54. Dunse, T.; Schuler, T.V.; Hagen, J.O.; Reijmer, C.H. Seasonal Speed-up of Two Outlet Glaciers of Austfonna, Svalbard, Inferred from Continuous GPS Measurements. *Cryosphere* **2012**, *6*, 453–466. [CrossRef]
55. How, P.; Benn, D.I.; Hulton, N.R.J.; Hubbard, B.; Luckman, A.; Sevestre, H.; van Pelt, W.J.J.; Lindbäck, K.; Kohler, J.; Boot, W. Rapidly Changing Subglacial Hydrological Pathways at a Tidewater Glacier Revealed through Simultaneous Observations of Water Pressure, Supraglacial Lakes, Meltwater Plumes and Surface Velocities. *Cryosphere* **2017**, *11*, 2691–2710. [CrossRef]
56. Łupikasza, E.B.; Ignatiuk, D.; Grabiec, M.; Cielecka-Nowak, K.; Laska, M.; Jania, J.; Luks, B.; Uszczyk, A.; Budzik, T. The Role of Winter Rain in the Glacial System on Svalbard. *Water* **2019**, *11*, 334. [CrossRef]

57. Davison, B.J.; Sole, A.J.; Cowton, T.R.; Lea, J.M.; Slater, D.A.; Fahrner, D.; Nienow, P.W. Subglacial Drainage Evolution Modulates Seasonal Ice Flow Variability of Three Tidewater Glaciers in Southwest Greenland. *J. Geophys. Res. Earth Surf.* **2020**, *125*, e2019JF005492. [CrossRef]
58. Howat, I.M.; Joughin, I.; Fahnestock, M.; Smith, B.E.; Scambos, T.A. Synchronous Retreat and Acceleration of Southeast Greenland Outlet Glaciers 2000–06: Ice Dynamics and Coupling to Climate. *J. Glaciol.* **2008**, *54*, 646–660. [CrossRef]
59. King, M.D.; Howat, I.M.; Candela, S.G.; Noh, M.J.; Jeong, S.; Noël, B.P.Y.; van den Broeke, M.R.; Wouters, B.; Negrete, A. Dynamic Ice Loss from the Greenland Ice Sheet Driven by Sustained Glacier Retreat. *Commun Earth Env.* **2020**, *1*, 1. [CrossRef]
60. Moon, T.; Joughin, I.; Smith, B. Seasonal to Multiyear Variability of Glacier Surface Velocity, Terminus Position, and Sea Ice/Ice Mélange in Northwest Greenland. *J. Geophys. Res. Earth Surf.* **2015**, *120*, 818–833. [CrossRef]
61. Podrasky, D.; Truffer, M.; Fahnestock, M.; Amundson, J.M.; Cassotto, R.; Joughin, I. Outlet Glacier Response to Forcing over Hourly to Interannual Timescales, Jakobshavn Isbræ, Greenland. *J. Glaciol.* **2012**, *58*, 1212–1226. [CrossRef]
62. Pętlicki, M.; Ciepły, M.; Jania, J.A.; Promińska, A.; Kinnard, C. Calving of a Tidewater Glacier Driven by Melting at the Waterline. *J. Glaciol.* **2015**, *61*, 851–863. [CrossRef]
63. Truffer, M.; Motyka, R.J. Where Glaciers Meet Water: Subaqueous Melt and Its Relevance to Glaciers in Various Settings. *Rev. Geophys.* **2016**, *54*, 220–239. [CrossRef]
64. Colgan, W.; Rajaram, H.; Abdalati, W.; McCutchan, C.; Mottram, R.; Moussavi, M.S.; Grigsby, S. Glacier Crevasses: Observations, Models, and Mass Balance Implications. *Rev. Geophys.* **2016**, *54*, 119–161. [CrossRef]
65. Winsvold, S.H.; Kääb, A.; Nuth, C. Regional Glacier Mapping Using Optical Satellite Data Time Series. *IEEE J. Sel. Top. Appl. Earth Obs. Remote Sens.* **2016**, *9*, 3698–3711. [CrossRef]